Investigation and Analytical Description of Acoustic Production by Magneto-Acoustic Mixing Technology

HUNTER B. HENDERSON, ORLANDO RIOS, GERARD M. LUDTKA, and MICHELE V. MANUEL

Magneto-Acoustic Mixing Technology is a novel manufacturing method that combines two magnetic fields to produce high-intensity sonication for liquid-state materials processing. This method may be adapted to the manufacture of various materials that benefit from a combination of high temperature, magnetic fields, and acoustic energy. In this work, acoustic generation mechanisms are described in detail and found to be dependent on the skin depth of the induction currents. Analytical models of acoustic pressure are derived, based on two mutually exclusive vibration mechanisms, crucible and melt vibration. Additionally, grain size evidence of acoustic pressure distribution is presented as preliminary model validation.

DOI: 10.1007/s11663-015-0359-1
© The Minerals, Metals & Materials Society and ASM International 2015

I. INTRODUCTION

WITH increased demands for high-performance materials, there is a need for new fabrication methods that can create microstructures optimizing unique structure–property relationships.[1] Both magnetic and acoustic treatments of metals are gaining industrial relevance, as evidenced by the European Union-sponsored ExoMet Project that aims to improve the use of external fields in materials processing.[2–4] Processing materials under high magnetic fields have been shown to alter particle orientation and dispersion,[5,6] change solidification microtexture,[7,8] and modify microstructure and solute distribution through damped convection.[9–11] Acoustic processing, on the other hand, has been shown to improve reactivity,[12,13] disperse nanoparticles,[14–16] and refine solidification microstructures.[17,18] This work focuses on Magneto-Acoustic Mixing Technology (MAMT), which has the potential to effect material structures through the simultaneous application and coupling of magnetic and induction fields to produce strong, yet, controlled acoustic waves in a melt.[19,20] Full utilization of the technology requires a fundamental understanding of inherent, operant mechanisms and associated interactions, as well as careful design of system components. This work provides a fundamental understanding of the underlying physics that control the performance of the system and the materials that are processed by it.

The key components of an MAMT system are the presence of a strong static magnetic field and an induction coil assembly. When combined in an orthogonal geometry, this system provides both heating and acoustic power to a metallic melt housed in an internal crucible. An illustration is shown in Figure 1(a). The induction system induces electric eddy currents in the liquid metal and crucible. These currents (blue) increase the temperature by Joule heating, a primary mechanism of induction heating.[21] Additionally, these eddy currents couple with the static magnetic field (red) to produce an alternating Lorentz force (green) that displaces the liquid, generating acoustic waves at the induction frequency. If the system is configured in a cylindrical configuration, the acoustic waves propagate in a radial direction in the crucible wall and sample. Photographs of the magnet and installed system are shown in Figures 1(b) and 1(c).

Magneto-Acoustic Mixing Technology is a subset of Electromagnetic Acoustic Transduction (EMAT), in which electromagnetic energy is converted into acoustic energy. Conventional EMAT has been traditionally used for non-destructive evaluation. MAMT can be distinguished from conventional EMAT in geometry and the level of power supplied.[20] Another key difference is the nature of the acoustic wave that is produced. As shown in Figure 2, MAMT produces longitudinal waves, whereas conventional EMAT induces shear waves. The fact that MAMT produces longitudinal waves is of key importance since shear waves require a rigid body through which to propagate,[22] making them ineffective for liquid processing. Additionally, the presence of the high magnetic field dramatically reduces the need for large eddy currents, allowing electromagnetic induction to be used as the current source in a non-contact fashion while still producing significant acoustic vibration in the sample. It is the maturation of superconducting magnetics that enables this technology as

HUNTER B. HENDERSON, Postdoctoral Associate, and MICHELE V. MANUEL, Associate Professor, are with the Department of Materials Science and Engineering, University of Florida, 100 Rhines Hall, P.O. Box 116400, Gainesville, FL 32611. Contact e-mail: mmanuel@mse.ufl.edu ORLANDO RIOS, Associate Research Staff, is with the Deposition Sciences Group, Oak Ridge National Laboratory, 1 Bethel Valley Road, Oak Ridge, TN, and also Adjunct Professor, with the Department of Materials Science and Engineering, University of Tennessee, Oak Ridge National Laboratory. GERARD M. LUDTKA, Distinguished R&D Staff, is with the Materials Science & Technology Division, Oak Ridge National Laboratory.
Manuscript submitted May 4, 2014.
Article published online May 7, 2015.

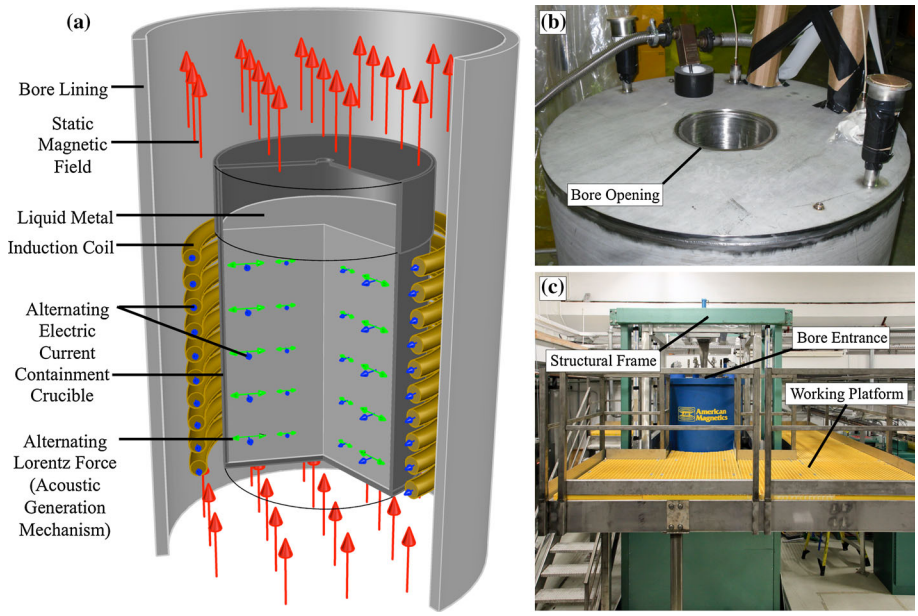

Fig. 1—(*a*) Cutaway schematic of an MAMT system. (*b*) Entrance to ORNL's 200 mm warm bore magnet in which an induction coil and sample holder is housed. (*c*) Fully assembled magnet with elevated work platform.

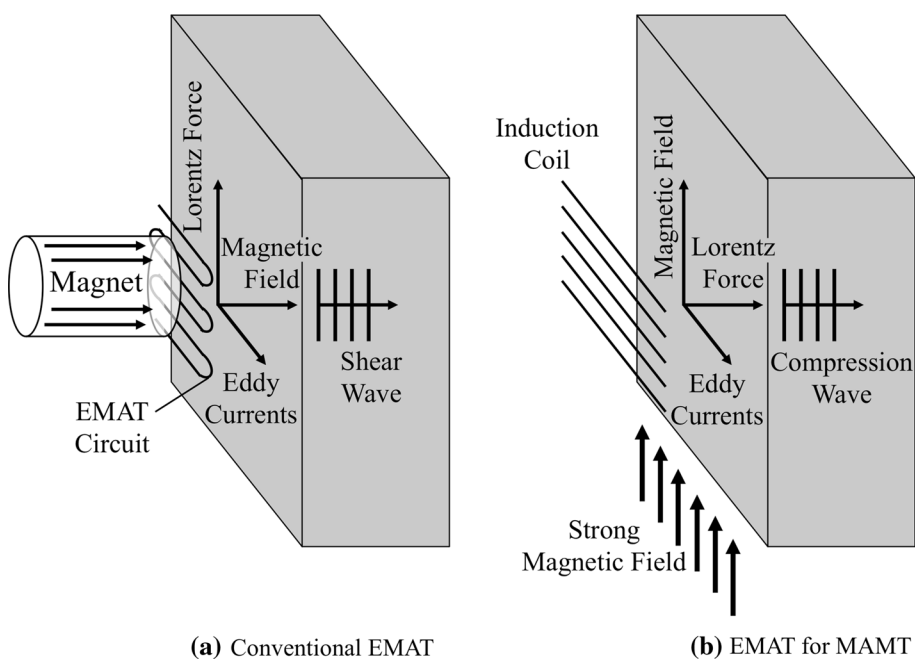

Fig. 2—Comparison between (*a*) conventional EMAT typically used for non-destructive evaluation and (*b*) MAMT system for materials processing.

magnetic fields of high strength (>5 T) have become routinely available,[23] increasing the potential sonic intensity for materials processing.

Another variant of EMAT technology, which has analogs to MAMT is Electromagnetic Vibration (EMV).[24,25] Similar to MAMT, EMV utilizes the Lorentz forces to create acoustic waves to process liquids. These forces are generated when alternating electric current applied by graphite electrodes in contact with the sample couple with a transverse static magnetic field. The use of contacting electrodes differentiates EMV from MAMT. MAMT is a contactless technique, whereby the sample itself and sample container generate acoustic waves. EMV relies on the electrodes being in direct contact with the melt,[25,26] which makes electrode contamination a possibility and hinders the scalability and flexibility in manufacturing practices.

This work focuses on the dominant physical mechanisms in the MAMT system. First, magnetic and acoustic mechanisms that may be active in a material being

treated with MAMT are explored. Next, the importance of skin depth and its implications on acoustic generation in MAMT are described, theoretical descriptions are derived and then compared with some experimental evidence. Taken together, the reader should become familiar with the potential uses of MAMT and gain a solid framework for its implementation.

II. PRINCIPAL PHYSICAL MECHANISMS DRIVING PERFORMANCE

Acoustic treatment is used in numerous scientific applications and involves the production and propagation of mechanical waves through a material. A common use is in non-destructive evaluation of components, in which scattering of sonic waves from defects is measured.[27,28] In contrast, high-intensity fields (typically above 100 W/cm^2) are used in many materials processing applications[29] such as refining solidification microstructures, sonochemistry, and melt-degassing, all of which occur in the liquid state.

In liquids, wave speed (c) can be calculated through the use of Eq. [1] where β_{ad} is the adiabatic compressibility and ρ is the density.[29] For longitudinal waves, amplitude can also be the pressure variation between compression and rarefaction regions of the wave. Additionally, maximum acoustic pressure (P_A) and intensity (I) can be calculated by Eqs. [2] and [3],[29] where A_0 is the maximum particle displacement (how far particles in the liquid move as a result of wave propagation) and f is frequency. Acoustic pressure and intensity are necessary to understand whether the cavitation threshold, corresponding to the rapid growth and collapse of vacuum bubbles in the liquid, has been reached in a fluid.[30,31] Acoustic pressure is the deviation from atmospheric pressure, and acoustic intensity is defined as sound power per unit area.

$$c = \sqrt{\frac{1}{\beta_{ad} \cdot \rho}} \quad [1]$$

$$P_A = 2\pi\rho c A_0 f \quad [2]$$

$$I = 2\rho c(\pi A_0 f)^2 \quad [3]$$

The presence of cavitation bubbles can dramatically affect physical processes in the liquid and during solidification.[32] As cavitation bubbles collapse, the local area experiences extreme pressure and temperature fluctuations (low estimates are 5000 K and 100 atm[33]). These local "hot spots" can act as nucleation or reaction sites for numerous mechanisms, forming the basis for the field of sonochemistry. The spontaneous formation of cavitation can occur homogeneously, but in practice most cavitation occurs heterogeneously at small gas pockets or interfaces.[34] An important effect of cavitation is microjet formation, in which a cavitation bubble collapses asymmetrically near an interface and a jet of liquid is driven at high speed into the interface.[35] This jet can reach hundreds of meters per second, enhancing the wettability of particles and surface reactions.[12]

During melt processing in a magnetic field, magnetohydrodynamics (MHD) can dominate the behavior of conductive fluids.[36–38] When free electrons in the conductive melt cross magnetic field lines, they induce local eddy currents that in turn restrict further movement.[37] This phenomenon results in conductive fluids being "tied" to magnetic field lines, *i.e.,* a portion of a conductive fluid may travel along a field line unhindered, but is restricted from crossing field lines. The most prevalent effect for metallic melts in a magnetic field is an increase in apparent melt viscosity.[39] This results in reduced bulk motion of the conductive fluid, advection, often changing the solidification behavior of metals significantly.[40]

The combination of magnetic fields, acoustic power, and temperature control enables a number of unique experimental approaches. First, the damped convection caused by the magnetic field allows for fundamental studies on solidification behavior. Damped convection limits the remelting and transport of dendrite arms, a primary mechanism of equiaxed grain production,[41] and would promote columnar growth.[42] Limiting convection would also reduce macrosegregation of solutes.[43]

III. SKIN DEPTH EFFECTS

In the current geometry of liquid in a cylindrical container, MAMT acoustic wave production may proceed by two vibration mechanisms: (1) using the crucible as an acoustic source (crucible vibration) or (2) directly vibrating the melt (melt vibration). The dominate mechanism is determined by the skin effect.[44] When an alternating current travels in a conductor, the current density is the highest on the surface because of internally induced current loops that in turn oppose bulk current flow. The current density drops exponentially away from the surface, by the relation in Eq. [4], in which J is the current density [A/m^2] at depth d, J_s is the surface current density [A/m^2], and δ is the skin depth.[45] The skin depth is the depth from the surface at which the current density has dropped to $1/e$ (or ~37 pct) of the surface value, which is described in Eq. [5], where ρ_r is resistivity, f is the alternating current frequency, μ_0 is the permeability of free space, and μ_r is the relative permeability of the conductor.[45] Thus, 63 pct of the current is within the skin depth. This factor determines whether the major vibration source is the melt or crucible (shown schematically in Figure 3).

$$J = J_s e^{-d/\delta} \quad [4]$$

$$\delta = \sqrt{\frac{\rho_r}{\pi f \mu_0 \mu_r}} \quad [5]$$

The process of acoustic production for each of the vibration mechanisms is quite distinct. In crucible vibration, the entire crucible expands and contracts, so

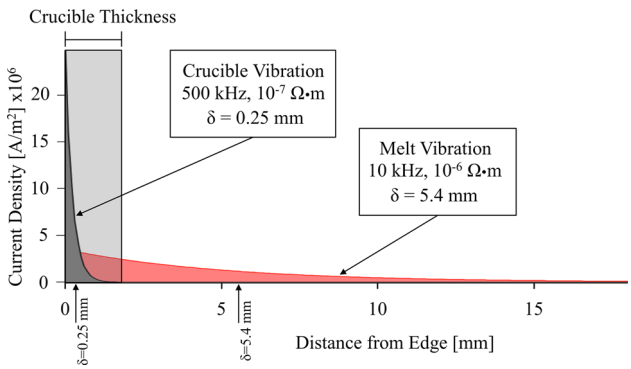

Fig. 3—Distribution of eddy currents for two situations, melt vibration seen in the current studies, and a crucible vibration, obtained by varying frequency and crucible resistivity. The resistivity values were chosen to illustrate the two vibration mechanisms on a singular plot.

the displacement is dependent on the total induction current in the crucible and the crucible thickness. As the crucible vibrates, it acts as an acoustic source at the crucible/melt interface, and acoustic waves produced at the interface will propagate inward. This can be contrasted with melt vibration, where acoustic intensity is dependent on the local induction current density in the liquid,[25] and thus the sound is produced in a delocalized fashion throughout the liquid. For example, for the melt vibration mechanism shown in Figure 3, the acoustic generation would be higher at a distance of 2 mm than 8 mm. It should be noted that there are limits to how large the skin depth can be for effective MAMT treatment. If the skin depth is too large, eddy currents will overlap, negating each other, due to the cylindrical nature of the system geometry.[45] Since skin depth is dependent on frequency and the properties of the crucible and melt, these factors should be considered to control for acoustic performance.

In order to transition from a melt to crucible vibration, the total current in the workpiece must be examined so as to avoid extending the induced current beyond the thickness of the crucible. This is accomplished by multiplying the current by the cumulative distribution function of the skin depth, or the fraction of total current within a certain depth. The cumulative distribution function of a negative exponential such as Eq. [4] is given in Eq. [6], with depth d and skin depth δ. If crucible thickness is substituted for d, then Eq. [6][46] gives the fraction of the total current in the crucible.

$$F(d;\delta) = 1 - \mathrm{e}^{-d/\delta} \qquad [6]$$

Next, two analytical models are developed that describe acoustic production based on induction current in the crucible or melt. The percentage of induction current in the crucible from Eq. [6] indicates which model is most appropriate. One necessary quantity needed for the models is the total induction current. Since the induction coil is helical and the workpiece is cylindrical, this may be done following the transformer equations for induction heating. Equation [7][45] describes the current in the workpiece I_w, the number of turns in the induction coil N_c, and the current in the coil I_c.

$$I_\mathrm{w} = I_\mathrm{c} N_\mathrm{c} \qquad [7]$$

IV. MODEL 1: MELT VIBRATION

As shown in Figure 3, the active mechanism depends on the location of the induced current, whether it lies in the crucible or the melt. If the induced current is located primarily in the melt, the system is considered to be in melt vibration. In order to mechanistically explore the relationship between the physics, material properties, and resultant acoustic behavior, a simplified model is derived.

Before the acoustic pressure due to melt vibration can be calculated, the distribution of induced current density in the melt must be determined. First, the surface current density, J_s, from Eq. [4] will be calculated. Taking the integral of Eq. [4] from 0 to ∞ and multiplying by the height of the workpiece (h_w) gives the total current in Eq. [8]. Rearranging Eq. [8] gives the surface current density in terms of induction and material parameters (Eq. [9]). At this point, the skin depth used is that for the metallic melt, not the crucible.

$$h_\mathrm{w} \int_0^\infty J_\mathrm{s} \mathrm{e}^{-d/\delta} \mathrm{d}d = -h_\mathrm{w} J_\mathrm{s} \delta \mathrm{e}^{-d/\delta} \Big|_0^\infty = h_\mathrm{w} J_\mathrm{s} \delta = I_\mathrm{w} \qquad [8]$$

$$J_\mathrm{s} = \frac{I_\mathrm{w}}{h_\mathrm{w}\delta} = \frac{I_\mathrm{c} N_\mathrm{c}}{h_\mathrm{w}\delta} \qquad [9]$$

The local particle acceleration (a) due to the Lorentz force is given in Eq. [10], where J is the current density, B_0 is the magnetic flux density, and ρ_l is the density of the melt.[25] Particle acceleration may be related to acoustic pressure p_ac by Eq. [11], where c is the speed of sound in a liquid, β_ad is the melt adiabatic compressibility, and f is the frequency.[29] Because pressure is directly dependent on the current density, it will decrease away from the edge as a consequence of the skin effect.

$$a = \frac{JB_0}{\rho_\mathrm{l}} \qquad [10]$$

$$p_\mathrm{ac} = \frac{\mathrm{ac}\rho_l}{2\pi f} = \frac{a}{2\pi f}\sqrt{\frac{\rho_\mathrm{l}}{\beta_\mathrm{ad}}} \qquad [11]$$

The final expression for acoustic pressure, assuming melt sonication, is given in Eq. [12], a combination of Eqs. [4], [9], [10], and [11]. It can be seen that the pressure is proportional to both the induction current and the static field. The influence of relative permeability is minimal for liquid metals, since they are non-ferromag-

netic, with μ_r very close to 1. This will change for liquids containing ferromagnetic particles, however. The pressure is inversely proportional to the square root of frequency, so, as frequency decreases, pressure increases. Lowering the frequency will not increase the pressure without limit. A lower frequency will increase the skin depth, and if the skin depth approaches the radius of the workpiece, induction (and therefore EMAT) becomes much less effective.[45] Sound pressure can be related to acoustic intensity (I_{ac}) by Eq. [13].[29]

$$p_{ac}(d) = \frac{I_w B_0}{2\pi f \delta h_w} \sqrt{\frac{1}{\rho_l \beta_{ad}}} e^{-d/\delta} \quad [12]$$

$$I_{ac} = \frac{p_{ac}^2}{\rho_l c} \quad [13]$$

Experimental evidence in support of the melt vibration model was obtained by observing grain refinement as a function of distance from the crucible wall under MAMT, since it has been well documented that grain size reduction scales with acoustic energy delivered during solidification.[30,47–50] The critical component of grain refinement is the presence of acoustic cavitation, which is dependent on the acoustic pressure of waves in a liquid. The acoustic pressure above which cavitation occurs is called the cavitation threshold and is usually 0.5 to 1.0 MPa for light alloy melts.[29,32] The current material being investigated is pure Mg inoculated with 1 vol pct Dy_2O_3 nanoparticles. The Dy_2O_3 inoculant reduces the cavitation threshold to below 0.5 MPa,[29] making the threshold more predictable than without an inoculant. This sample was solidified in a 30 mm diameter, 0.5 mm thick stainless steel crucible under a 20 T field with a 10 kHz induction field active to a skin depth of 5.4 mm. The sample was gas quenched, so solidified from the outside in. More specific information regarding the processing conditions is discussed elsewhere.[20] The grain size of the cast material, along with the distribution of acoustic pressure in the melt from Eq. [12], can be seen in Figure 4. The sample solidified inward from the edge, so the maximum acoustic pressure available in the melt corresponds to the acoustic pressure at the solid–liquid boundary (*e.g.,* when the sample had solidified 4 mm inward, the maximum acoustic pressure was 1 MPa). It can be seen in Figure 4 that, as the acoustic pressure drops below the cavitation threshold, the grain size increases dramatically. This indicates that Eq. [21] is accurate in predicting which areas of the melt experience cavitation, given the specific set of process variables. The black particles visible in Figure 4 are primarily Dy_2O_3 and did not contribute to the transition in grain size, since they were found in equal area fractions throughout the microstructure. These results can be compared to pure Mg samples solidified under no field and only an 18 T field, both of which exhibited columnar grains greater than 2 mm in diameter.[20] Thus, the acoustic field was primarily responsible for grain refinement. Further studies are needed to determine if Eq. [12] is accurate across a range of materials (with different resistivity and density) and process inputs (like frequency, field strength, and crucible size).

V. MODEL 2: CRUCIBLE VIBRATION

The second model assumes that all induction current is contained within the crucible walls and depends largely on the geometric and elastic properties of the crucible. Several assumptions are made in the model. The first is

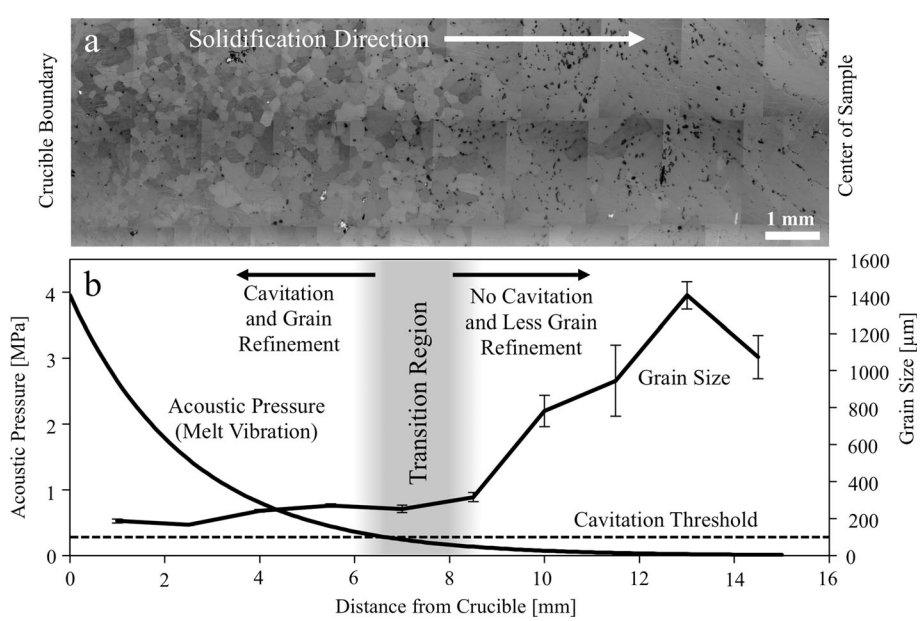

Fig. 4—(*a*) Microstructure and (*b*) grain size and calculated acoustic pressure in Mg-Dy_2O_3 processed by MAMT. The region in which acoustic pressure was greater than the cavitation threshold has refined grains.

that the contained liquid and containment crucible are in constant contact. Because of this, physical interactions of the melt with the container (damping) are ignored. Second, the alternating eddy currents and resultant "flexing" of the container by the Lorentz force are presumed to be in phase. At high frequencies, both of these assumptions will fail as inertial effects become more dominant. For this calculation, all induction eddy currents are assumed to be in the crucible, so currents within the melt are neglected for analytical simplicity.

First, the distribution of eddy currents in the crucible will be calculated based on transformer equations and skin depth. Second, the body forces due to the Lorentz interaction are calculated. The subsequent deformation of the container is determined, and its amplitude is related to sound intensity. For the calculation of container deformation, the container is idealized as an unbound cylinder for simplicity. An actual container is likely to be bound on one side and consequently stiffer; in this case, the calculated displacement amplitude will be an over-estimate.

Having described the distribution of current, the Lorentz force due to the interaction of current and static field is calculated. Equation [14] gives the vector form of the Lorentz force F_L, where I is the current, B_0 is the magnetic flux density, and the integral is with respect to traveled distance c.[51] dc is an infinitesimal circumferential distance over which the current travels. Because c and B_0 are always perpendicular (B_0 is in the axial direction of the cylinder), the cross product in Eq. [14] can be transformed into a direct multiplication in Eq. [15]. The total force on the cylinder toward the central axis of the cylinder (F_{tot}) is now calculated by integrating Eq. [15] from 0 to C_w. This resulting total force is given in Eq. [16].

$$\boldsymbol{F}_L = \int I(\mathrm{d}\boldsymbol{c} \times \boldsymbol{B}_0) \quad [14]$$

$$\boldsymbol{F}_L = \int I\boldsymbol{B}_0 \mathrm{d}\boldsymbol{c} \quad [15]$$

$$F_{tot} = I_{cr} C_w B_0 \quad [16]$$

The total body force due to the Lorentz interaction may be converted to and visualized as a pressure for ease of analysis. This "pseudopressure" acts similarly to an alternating hydrostatic pressure on the container and is calculated by dividing F_{tot} by the external induction area of the crucible, $C_w h_w$, in Eq. [17]:

$$p_{pseudo} = \frac{F_{tot}}{h_w C_w} = \frac{I_{cr} C_w B_0}{h_w C_w} = \frac{I_{cr} B}{h_w}. \quad [17]$$

Next, the deflection of the crucible from this pressure must be calculated. Equation [18] gives the radial displacement of a cylinder δ_r, as a function of pressure p, radius r, Young's modulus E, and thickness t.[52] Substituting Eq. [17] into [18] gives Eq. [19].

$$\delta_r = \frac{pr^2}{Et} \quad [18]$$

$$\delta_r = \frac{I_{cr} B_0 r^2}{E h_w t} \quad [19]$$

As previously mentioned, an assumption made for this model is constant contact between the crucible and liquid. If this is the case, then the crucible displacement is equal to the local particle displacement in the liquid ξ in Eq. [20]:

$$\delta_r = \xi = \frac{I_{cr} B_0 r^2}{E h_w t}. \quad [20]$$

Particle displacement ξ may be related to acoustic pressure (p_{ac}) as Eq. [21], where ρ_l is the density of the fluid, c is the speed of sound (Eq. [1]) in the fluid, f is the frequency of the sound (equivalent to the induction frequency),[29] and β_{ad} is the fluid adiabatic compressibility.

$$p_{ac} = 2\pi\rho_l c f \xi = 2\pi f \xi \sqrt{\frac{\rho_l}{\beta_{ad}}} \quad [21]$$

Substituting Eq. [20] into Eq. [21] gives the acoustic pressure at the crucible–melt boundary in Eq. [22]:

$$p_{ac} = \frac{2\pi f I_{cr} B_0 r^2}{E h_w t} \sqrt{\frac{\rho_l}{\beta_{ad}}}. \quad [22]$$

Based on Eqs. [12] and [22], frequency has a dominant effect on the acoustic pressure. The previous models did not account for inertia-limited displacement that occurs at high frequency, however. At low harmonic loading frequencies, an elastic material deforms proportionally to the applied load. Conversely, at higher frequencies, a phase lag between the load and displacement reduces the magnitude of oscillation as inertial forces become more dominant.[53] The current experimental setup precluded experimental study of crucible vibration (Eq. [22]), but this model could be useful for designing apparatuses for the treatment of non-conductive liquids, such as in aqueous systems.

VI. CONCLUSIONS

MAMT, a non-contact acoustic processing technology developed using a high magnetic field in conjunction with induction heating, has significant promise in impacting commercial casting applications with the potential to apply heat, magnetic fields, and acoustic energy to achieve novel material structures. Using a high-field MAMT method, non-contacting ultrasonic treatment can be applied to the processing of metal alloys in either the solid or liquid phase. Molten metals can be contained in crucibles that are readily penetrated by the electromagnetic induction fields. The skin depth of induction currents is a vital aspect of vibration production in an MAMT system, determining whether melt or crucible vibration is more active.

Models of acoustic production for both conditions were developed and presented. In comparing the two models, it is clear that the mechanics of acoustic production are quite distinct. For crucible vibration, the source of acoustic waves is discrete at the crucible–melt interface, as opposed to being delocalized for melt vibration. Crucible vibration depends on extrinsic and intrinsic properties of the crucible, but especially thickness and radius. Melt vibration, on the other hand, depends greatly on the conductivity of the liquid. The resultant effects of this mechanism were clearly demonstrated in an Mg-Dy_2O_3 casting. Frequency affects the two models differently as well, but inertial effects will eventually restrict acoustic production by both mechanisms. Both pressure models scale with induction current density and magnetic flux density of the static field, meaning that high acoustic pressures can be achieved by increasing either of these parameters. The two models developed in this work form a theoretical basis on which future MAMT studies can be based, elucidating under which conditions acoustic cavitation would be expected. At intermediate skin depths, in which a considerable percentage of induction currents are in the crucible and melt, the mechanics of acoustic production will be more complicated. This is because a phase lag between the melt and crucible could cause impacts and shock waves to propagate from the interface. Numerical multiphysics models will likely be able to more accurately represent the physics in the system[54–56] and should be pursued in future studies.

While MAMT possesses the unique ability to apply heat, magnetic fields, and acoustic fields, there are challenges that must be overcome prior to widespread industrial use. First, since a large bore superconducting magnet is required for high magnetic fields, an application that warrants the capital expenditure must be identified. One possibility could be a high-throughput liquid metal treatment in a pipe, for instance. Second, any acoustic resonances of the crucible and insulation would need to be identified and mitigated. Conversely, resonance of the crucible could be exploited to increase acoustic intensity in crucible vibration. Careful consideration of induction power, magnetic field strength, material conductivity, and system dimensions should be used when evaluating the applicability of MAMT.

ACKNOWLEDGMENTS

The authors would like to thank Dr. Zachary L Bryan for his experimental support and Professors Curtis Taylor and Simon Phillpot for their thoughtful comments. The authors acknowledge support by the Advanced Manufacturing Office (AMO) in the Office of Energy Efficiency and Renewable Energy (EERE), as part of the Department of Energy (DOE). Facilities were provided by the Manufacturing Demonstration Facility (MDF) at Oak Ridge National Laboratory (ORNL). This material is based upon work supported by the National Science Foundation under grant numbers DMR-0845868. The research sponsored was in part by the U.S. Department of Energy, Office of Energy Efficiency and Renewable Energy, Advanced Manufacturing Office, under contract DE-AC05-00OR22725 with UT-Battelle, LLC.

REFERENCES

1. W.J. Joost: *JOM*, 2012, vol. 64, pp. 1032–38.
2. N. Hari Babu, Z. Fan, and D.G. Eskin: in *TMS2013 Annual Meeting Supplemental Proceedings*, San Antonio, TX, 2013, pp. 1037–44.
3. H. Emmerich, H. Lowen, R. Wittkowski, T. Gruhn, G.I. Toth, G. Tegze, and L. Granasy: *Adv. Phys.*, 2012, vol. 61, pp. 665–743.
4. W.H. Sillekens, D.J. Jarvis, A. Vorozhtsov, V. Bojarevics, C.F. Badini, M. Pavese, S. Terzi, L. Salvo, L. Katsarou, and H. Dieringa: *Metall. Mater. Trans. A-Phys. Metall. Mater. Sci.*, 2014, vol. 45A, pp. 3349–61.
5. P. Gillon: *Mater. Sci. Eng. A-Struct. Mater. Prop. Microstruct. Process.*, 2000, vol. 287, pp. 146–52.
6. S. Asai: *Model. Simul. Mater. Sci. Eng.*, 2004, vol. 12, pp. R1–12.
7. M.J. Li, T. Tamura, and K. Miwa: *Metall. Mater. Trans. A*, 2009, vol. 40A, pp. 1422–35.
8. T. Sugiyama, M. Tahashi, K. Sassa, and S. Asai: *ISIJ Int.*, 2003, vol. 43, pp. 855–61.
9. S. Yang, W.J. Liu, and J. Jia: *J. Mater. Sci.*, 2001, vol. 36, pp. 5351–55.
10. Q. Wang, D.G. Li, K. Wang, Z.Y. Wang, and J.C. He: *Scripta Mater.*, 2007, vol. 56, pp. 485–88.
11. X. Li, Z.M. Ren, and Y. Fautrelle: *J. Cryst. Growth*, 2006, vol. 290, pp. 571–75.
12. K.S. Suslick and G.J. Price: *Annu. Rev. Mater. Sci.*, 1999, vol. 29, pp. 295–326.
13. A. Gedanken: *Ultrason. Sonochem.*, 2004, vol. 11, pp. 47–55.
14. M. De Cicco, H. Konishi, G.P. Cao, H.S. Choi, L.S. Turng, J.H. Perepezko, S. Kou, R. Lakes, and X.C. Li: *Metall. Mater. Trans. A*, 2009, vol. 40A, pp. 3038–45.
15. K.B. Nie, X.J. Wang, K. Wu, L. Xu, M.Y. Zheng, and X.S. Hu: *J. Alloy. Compd.*, 2011, vol. 509, pp. 8664–69.
16. Y. Yang and X.C. Li: *J. Manuf. Sci. Eng.-Trans. ASME*, 2007, vol. 129, pp. 252–55.
17. M. Qian, A. Ramirez, and A. Das: *J. Cryst. Growth*, 2009, vol. 311, pp. 3708–15.
18. M. Li, T. Tamura, and K. Miwa: *Acta Mater.*, 2007, vol. 55, pp. 4635–43.
19. R. Jaramillo, R. Kisner, Ge. Ludtka, Ga. Ludtka, and J. Wilgen: USA Patent 7534980, 2009.
20. H.B. Henderson, O. Rios, Z.L. Bryan, C.P. Heitman, G.M. Ludtka, G. Mackiewicz-Ludka, A.M. Melin, and M.V. Manuel: *Adv. Eng. Mater.*, 2014, vol. 16, pp. 1076–82.
21. J.S. Park, S. Taniguchi, and Y.J. Park: *J. Phys. D-Appl. Phys.*, 2009, vol. 42, p. 6.
22. P.M. Shearer: *Introduction to Seismology*, 2nd ed., Cambridge University Press, Cambridge, 2009.
23. Q.L. Wang, L.G. Yan, B.Z. Zhao, S.S. Song, Y.Z. Lei, and I.E.E.E.T. Appl: *Supercon.*, 2004, vol. 14, pp. 372–75.
24. C. Vivés: *Metall. Mater. Trans. B*, 1996, vol. 27B, pp. 457–64.
25. C. Vivés: *Metall. Mater. Trans. B*, 1996, vol. 27B, pp. 445–55.
26. M.J. Li, T. Tamura, N. Omura, and K. Miwa: *J. Alloy. Compd.*, 2010, vol. 494, pp. 116–22.
27. L. Cartz: *Nondestructive Testing: Radiography, Ultrasonics, Liquid Penetrant, Magnetic Particle, Eddy Current*, ASM International, 1995.
28. M.V. Brook: *Ultrasonic Inspection Technology Development and Search Unit Design: Examples of Practical Applications*, Wiley-IEEE Press, New York, 2011.
29. G.I. Eskin: *Ultrasonic Treatment of Light Alloy Melts*, Gordon and Breach Science Publishers, Amsterdam, 1998.
30. L. Nastac: *Metall. Mater. Trans. B*, 2011, vol. 42B, pp. 1297–305.
31. M.S. Plesset and A. Prosperetti: *Annu. Rev. Fluid Mech.*, 1977, vol. 9, pp. 145–85.
32. G.I. Eskin: *Adv. Perform. Mater.*, 1997, vol. 4, pp. 223–32.

33. H.G. Flynn: *J. Acoust. Soc. Am.*, 1975, vol. 58, pp. 1160–70.
34. G.I. Eskin: *Ultrason. Sonochem.*, 1995, vol. 2, pp. S137–41.
35. T.B. Benjamin and A.T. Ellis: *Philosophical Transactions of the Royal Society of London Series a-Mathematical and Physical Sciences*, 1966, vol. 260, pp. 221–40.
36. J.C.R. Hunt and J.A. Sherclif: *Annu. Rev. Fluid Mech.*, 1971, vol. 3, pp. 37–62.
37. K.R. Cramer and S.-I. Pai: *Magnetofluid Dynamics for Engineers and Applied Physicists*, Scripta Publishing Company, USA, 1973.
38. P.A. Davidson: *An Introduction to Magnetohydrodynamics*, Cambridge University Press, Cambridge, 2001.
39. D.H. Matthiesen, M.J. Wargo, S. Motakef, D.J. Carlson, J.S. Nakos, and A.F. Witt: *J. Cryst. Growth*, 1987, vol. 85, pp. 557–60.
40. T. Emi and H. Shibata: in *Solidification and Casting*, B. O'Reilly and K. Cantor, eds., Institute of Physics Publishing, London, 2003, pp. 286–88.
41. H. Esaka, T. Wakabayashi, K. Shinozuka, and M. Tamura: *ISIJ Int.*, 2003, vol. 43, pp. 1415–20.
42. B.Q. Li: *JOM*, 1998, vol. 50, pp. 1–13.
43. D. Samanta and N. Zabaras: *Int. J. Heat Mass Transf.*, 2006, vol. 49, pp. 4850–66.
44. H.W. Deng, Y.J. Zhao, C.J. Liang, W.S. Jiang, and Y.M. Ning: *Prog. Electromagn. Res. M*, 2009, vol. 9, pp. 1–8.
45. P.G. Simpson: *Induction Heating: Coil and System Design*, McGraw-Hill, New York, 1960.
46. A. Gupta: *Risk Management and Simulation*, CRC Press, Boca Raton, FL, 2013.
47. Y. Mizutani, J. Kawata, K. Miwa, K. Yasue, T. Tamura, and Y. Sakaguchi: *J. Mater. Res.*, 2004, vol. 19, pp. 2997–3003.
48. M.J. Li, T. Tamura, N. Omura, and K. Miwa: *J. Alloy. Compd.*, 2009, vol. 487, pp. 187–93.
49. M.J. Li, T. Tamura, and K. Miwa: *J. Mater. Res.*, 2009, vol. 24, pp. 145–55.
50. G.I. Eskin: *Ultrason. Sonochem.*, 2001, vol. 8, pp. 319–25.
51. D.J. Griffiths: *Introduction to Electrodynamics*, Prentice-Hall, USA, 1999.
52. W. Young and R. Budynas: *Roark's Formulas for Stress and Strain*, 7th ed., McGraw-Hill, New York, 2001.
53. F.E. Tse, I.E. Morse, and R.T. Hinke: *Mechanical Vibrations: Theory and Applications*, Allyn & Bacon, Boston, NY, 1978.
54. H.T. Zhang, H. Nagaumi, Y.B. Zuo, and J.Z. Cui: *Mater. Sci. Eng. A-Struct. Mater. Prop. Microstruct. Process.*, 2007, vol. 448, pp. 189–203.
55. K. McManus, A. Williams, M. Cross, N. Croft, and C. Walshaw: *Int. J. High Perform. C.*, 2005, vol. 19, pp. 1–27.
56. C. Bailey, P. Chow, M. Cross, Y. Fryer, K. Pericleous, and P. Roy: *Soc. A-Math. Phy.*, 1996, vol. 452, pp. 459–86.